RSC Advances

PAPER

View Article Online
View Journal | View Issue

Cite this: *RSC Adv.*, 2020, **10**, 5478

Superhydrophobic lotus-leaf-like surface made from reduced graphene oxide through soft-lithographic duplication†

Xiawei Yun, Zhiyuan Xiong, Yaning He and Xiaogong Wang *

In this work, reduced graphene oxide (RGO) was used as a material to fabricate superhydrophobic lotus-leaf-like surfaces through soft-lithographic duplication. In the process, a polydimethylsiloxane (PDMS) stamp was prepared by replica molding against the surfaces of fresh lotus leaves that functioned as masters. A dispersion of octadecylamine-modified reduced graphene oxide (ODA-RGO) in tetrahydrofuran (THF) was used as "ink". The lotus-leaf-like surfaces were fabricated by microcontact printing on the solid substrates. The results showed that due to the good processibility of the ODA-RGO dispersion, the printed layers display papillary micro/nano-structures with high fidelity to the surfaces of lotus leaves. The RGO-based lotus-leaf-like surfaces possess superhydrophobic characteristics with a water contact angle larger than 160° and the contact angle hysteresis less than 5°. Due to the excellent chemical stability of the RGO sheets, as-prepared surfaces show remarkable superhydrophobic stability. The lotus-leaf-like surfaces maintain the superhydrophobicity after heating treatment at 150 °C for 24 h or being exposed to corrosive solutions with different pH values for 12 h. The present findings prove that the RGO-based material is an ideal candidate for fabrication of environment-durable lotus-leaf-like surfaces, which can be expected to have applications in different areas.

Received 10th December 2019
Accepted 23rd January 2020

DOI: 10.1039/c9ra10373b

rsc.li/rsc-advances

1 Introduction

Superhydrophobic surfaces ubiquitously exist in nature, involving different parts of many creatures, such as leaves of plants (*e.g.* lotus, canna, ramie, and rice), butterfly wings and feathers of water fowls.[1–3] These superhydrophobic surfaces are typically characterized by a water contact angle larger than 150° and a water sliding angle smaller than 10°.[4–8] Among them, the lotus-leaf is most well-known for its non-wetting surface featuring unique hierarchical micro/nanoscale structures.[4] In recent years, lotus-leaf-like surfaces have inspired many investigations for the basic understanding and applications in different areas.[9–11] Nature tells us that building-up of hierarchical surface structures with low surface-free-energy matter is a very effective approach to form superhydrophobic surfaces.[12,13] Many researchers have endeavoured to develop various methods and materials to mimic the lotus-leaf-like structures to obtain the superhydrophobic surfaces.[14–19] The micron-scale structures on lotus leaves, *i.e.*, epidermal cells covered with the papillae, can be feasibly prepared with high fidelity by different microfabrication methods. On the other hand, the surface nanostructures from extracellular cuticles can only be laboriously mimicked by special methods, such as surface roughing treatments in following processes to obtain higher hydrophobicity.[4] Apart from the drawback of the multi-step procedure, the superhydrophobic stability of the fabricated lotus-leaf-like surfaces is usually unsatisfactory, especially under harsh conditions, such as being exposed to a corrosive liquid or heated to a high temperature.

Soft-lithography with a full range of elastomer-tool-based processing methods, such as microcontact printing (μCP), replica molding (REM), microtransfer molding (μTM), micromolding in capillaries (MIMIC), solvent-assisted micromolding (SAMIM) and other facile approaches, has been well established as one of the most widely used methodologies in microfabrication because of its simplicity, cost-effectiveness and scalability.[20–24] For a specific application to prepare lotus-leaf-like surfaces, the replica molding (REM) has been adopted to prepare replicas of the lotus-leaf surfaces with PDMS,[25] and microcontact printing has been performed by using stamps duplicated from lotus leaves and an "ink" of a polymer solution.[26] Although these studies prove the feasibility of the soft-lithography to prepare lotus-leaf-like surfaces, the prepared surfaces only exhibit the replicas of the micron-scale structures of the lotus leaves, and the nano-scale details of the original surfaces are more or less lost in the process. At the current state of the soft-lithographic approach, it is desirable to find suitable material that can be used to fabricate lotus-leaf-like surfaces

Laboratory of Advanced Materials (MOE), Department of Chemical Engineering, Tsinghua University, Beijing 100084, P. R. China. E-mail: wxg-dce@mail.tsinghua.edu.cn

† Electronic supplementary information (ESI) available. See DOI: 10.1039/c9ra10373b

with the hierarchical micro/nano-structures, moreover, to endow the super-hydrophobic surfaces with superior environmental and thermal stability.

Graphene, a two-dimensional (2D) crystal of sp^2 hybridized carbon atoms, has triggered huge research enthusiasm owing to its unique physical and chemical properties.[27–29] In recent years, graphene oxide (GO) and reduced graphene oxide (RGO) as graphene derivatives have been intensively investigated owing to their fascinating properties and feasibility for scalable production.[30–35] Single-layered GO nanosheets are typically obtained from complete exfoliation of graphite oxide through chemical methods.[36,37] GO is generally amphiphilic with the nonpolar hydrophobic regions of nanosheets and the hydrophilic regions from oxygenated defects, vacancies and edges,[33] which is not suitable to prepare superhydrophobic surface. On the other hand, RGO prepared from GO by reduction is hydrophobic, due to the recovery of the honeycomb carbon framework, for which hydrophobicity can be further enhanced by introducing alkyl and other hydrophobic groups on the nanosheets.[34,35] The anisotropic mechanical properties of RGO sheets, in-plane rigidity and out-of-plane flexibility, are beneficial to follow the topological profiles of elastomer tools. This property together with the good dispersion in suitable media make RGO be a unique candidate material for soft-lithographic patterning.[38] A surface with the nano-scale roughness is possible to be obtained through assembly and stacking of RGO nanosheets in the processing process. Moreover, the graphene-based materials is able to resist high temperatures and have proved to be able to prevent metal surfaces from oxidation and corrosion in the moist environment by coating on the surfaces.[39,40] Therefore, RGO can be ideal material used to prepare lotus-leaf-like surfaces through soft-lithography to ensure the high replica fidelity and superior stability. However, to our knowledge, a study employing RGO to fabricate lotus-leaf-like surfaces through soft-lithography has not appeared in the literature yet.

In this work, a soft-lithographic approach was developed to fabricate RGO-based lotus-leaf-like surfaces. In the process, PDMS stamps were prepared by the replica molding against the surfaces of fresh lotus leaves. The octadecylamine modified RGO (ODA-RGO) was prepared by chemical reduction of GO and surface modification. ODA-RGO was then dispersed in tetrahydrofuran (THF) to form the "ink". The lotus-leaf-like surfaces were fabricated by using the PDMS stamps and the "ink" through microcontact printing. The driving force and optimized conditions to transfer ODA-RGO nanosheets from the stamps to substrate surfaces were investigated. The obtained surfaces were proved to possess high fidelity to the original lotus leaves. The superhydrophobicity of the surfaces and its stability after heating treatment and exposure to corrosion media were investigated in detail.

2 Experimental section

2.1 Materials

The silicone elastomer kit was obtained from Dow Corning (Sylgard 184). The graphite powder (D_{50} < 600 nm, 99.95%) was purchased from Aladdin. Octadecylamine (ODA) was obtained from Sigma-Aldrich. Other chemicals and solvents were commercially purchased and used without further treatment. Ultrapure water (resistivity > 18.0 MΩ cm) was supplied by the Milli-Q water purification system and used for all experiments. The substrates (glass slides and silicon wafers) were treated with a piranha solution, obtained by mixing the concentrated sulphuric acid and hydrogen peroxide in a volume ratio of 3 : 1, then ultrasonically treated in the mixed solvents of water and acetone for about an hour, finally washed with acetone and carefully blown dry with air before use.

2.2 Synthesis of graphene oxide

Graphene oxide (GO) was obtained by oxidation of the graphite powder through the modified Hummers' method reported in the previous articles.[41,42] Typically, graphite (3.0 g) and potassium nitrate (3.6 g) were added into a 500 mL round-bottom flask, and then concentrated sulphuric acid (138 mL) was added into the flask cooling with an ice bath. The mixture was stirred for 30 min, followed by slow addition of potassium permanganate (18 g), when the temperature was kept below 5 °C. After that, the mixture was heated to 35 °C and stirred for 6 h. Ultrapure water (240 mL) was then slowly added into the mixture with the ice-bath cooling and the mixture was stirred for another 2 h. Then, an additional amount of ultrapure water (600 mL) was added, followed by dropwise addition of H_2O_2 (30%, 18 mL), during which the colour of the mixture turned from brown to yellow. After standing still for 12 h, the supernatant was decanted and sediment was repeatedly washed with water by centrifugation to remove residual metal oxides until the supernatant turned into neutral. The sediment was diluted with ultrapure water (2000 mL) and the dispersion was stirred for 24 h. Sequentially, the dispersion was treated by centrifugation at 6000 rpm for 5 min to remove the precipitate. The upper dispersion was then centrifuged at 18 000 rpm for 30 min and the supernatant was decanted. Finally, GO as the sediment was obtained, which could be easily dispersed in water with a high concentration by stirring.

2.3 Preparation of ODA-RGO dispersion

The octadecylamine modified reduced graphene oxide (ODA-RGO) was prepared by a reflux process as reported before.[43,44] GO dispersion (20 mg L^{-1}, 10 mL) was diluted with Ultrapure water (90 mL) under stirring and then ODA (200 mg, in 40 mL ethanol) was added dropwise into the solution. After refluxed at 90 °C for 48 h, hydroquinone (500 mg) was added to the mixture and reaction was carried out for another 24 h to achieve the effective reduction of GO. The reaction product was filtered, followed by washing with water and acetone each for three times. The black ODA-RGO powder was obtained after drying under vacuum at 60 °C for 24 h. Tetrahydrofuran (THF) was chosen as the dispersion medium of ODA-RGO due to its good volatility and excellent wettability to the PDMS stamps. In order to obtain an ODA-RGO sol both highly concentrated and well dispersed, a procedure of ultrasonic exfoliation, centrifugation and solvent evaporation was performed. ODA-RGO powder (50

mg) was dissolved in a centrifuge tube containing THF (30 mL) and ultrasonically treated for 3 h, followed by centrifuging at 3000 rpm for 30 min. The supernatant of the dispersion was poured into a beaker and the sediment was dispersed again with THF (30 mL). The ultrasound and centrifugation recycles were repeated until there was no residual sediment in the dispersion. After evaporating the solvent to the required volume at 80 °C, the dispersion was centrifuged at 1000 rpm for 5 min to remove large agglomerates. Finally, the highly concentrated ODA-RGO dispersion (1.67 mg mL^{-1}) was obtained and used as the "ink" for following contact printing experiment.

2.4 Preparation of lotus-leaf-like surfaces

The lotus-leaf-like surfaces were fabricated by microcontact printing with a special stamp prepared by duplication of the surface structures on the lotus leaves. In the process, a liquid prepolymer of polydimethylsiloxane (PDMS) was obtained by mixing the elastomer base and curing agent in a suitable proportion (10 : 1, wt/wt). A piece of the fresh lotus leaf was used as the master, after its surface was carefully cleared with deionized water and the surface moisture was removed by air dry. The prepolymer was poured on the leaf surface when it was kept in the turgor state. After curing in an oven at 50 °C for 6 h, the PDMS block was carefully peeled off from the mold and used as the stamp. A highly concentrated ODA-RGO dispersion in THF as the "ink" was added to cover the surface of the PDMS stamp through spreading. When the solvent almost volatilized by waiting for 10–20 s, the PDMS stamp was pressed against the substrate (glass slide and silicon wafer) on the surface for a few seconds (about 8–10 s) with gentle pressure. After the PDMS stamp was carefully peeled off, the substrate with the printed surface structure was kept in vacuum oven at 25 °C for 24 h.

2.5 Characterization

X-ray photoelectron spectroscopy (XPS) was carried out on an ESCALAB250Xi spectrometer with a monochromatized Al Kα X-ray source of 1486.6 eV. For the peak fitting, a linear background and fixed Gaussian–Lorentzian line shape with 20% Lorentzian were used for all spectra. X-ray diffraction (XRD) patterns were recorded on a Bruker D8 Advance X-ray diffractometer with Cu Kα radiation (1.5406 Å). Raman spectrum measurements were carried out on a Renishaw 1000 micro-spectrometer using an excitation wavelength of 514.5 nm. Fourier transform infrared (FTIR) spectra were measured on a Nicolet 560-IR spectrophotometer by incorporating the sample in the KBr pellet. Thermogravimetric analysis was carried out on TA Instruments TGA Q5000 with a heating rate of 10 °C min^{-1} under nitrogen atmosphere. An optical microscope (Olympus BH-2) was used for optical observation and photographic images were taken by using a digital camera (Nikon Coolpix E4500) connected to the microscope. Morphologies of all samples and energy-dispersive X-ray (EDX) analysis of the ODA-RGO surfaces were obtained by a field-emission scanning electron microscope (SEM) at 5.0 kV (Zeiss Merlin). The samples were sputtered with a thin layer of carbon before the SEM observation. Surface roughness of the samples was measured by the confocal microscope system (DCM8, Leica). The water contact angles were measured with a sessile drop method on a Dataphysics OCA-20 contact angle instrument and the measurement was carried out under air-ambient conditions with the droplet volume of 4 μL. The advancing and the receding water contact angles were also measured on the Dataphysics OCA-20 contact angle system by using a standard procedure. The data were obtained by first dropping 4 μL water on the surface and then injecting or retracting a water droplet (2 μL) through an automatic syringe in a rate of 0.6 μL s^{-1}. The sliding angle was calculated from the advancing and the receding water contact angles.

3 Results and discussion

In this study, reduced graphene oxide (RGO) was used as the basic material to fabricate the lotus-leaf-like surfaces through soft-lithography. Good wettability to the PDMS stamp and quick volatilization are the most important requirements for the solvent used in the contact printing. THF is a solvent that can well meet these requirements and was used here. In order to enhance the dispersion of the RGO nanosheets in THF, octadecylamine-modified reduced graphene oxide (ODA-RGO) was prepared by using method reported before.[43,44] After the functionalization and reduction, ODA-RGO with ODA grafts on the RGO surface is hydrophobic and suitable for the microcontact printing.

3.1 Characterization of ODA-ROD

Fig. 1a shows the FTIR spectra of GO, ODA and ODA-RGO, which indicate the successful preparation of RGO sheets with the ODA grafts. The FTIR spectrum of the GO shows a broad absorption band at 3300 cm^{-1}, which is assigned to the vibration of the OH groups. The bands peaked at 1631 cm^{-1} and

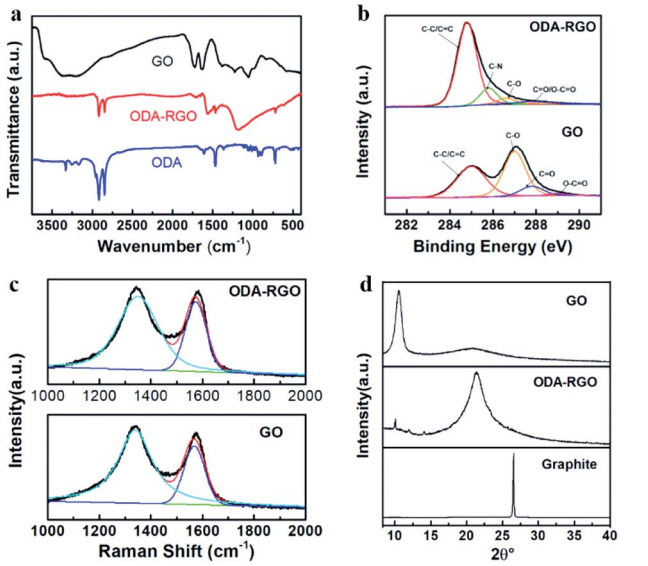

Fig. 1 Characterization of the ODA-RGO: (a) FTIR spectra of GO, ODA, and RGO-ODA. (b) C1s XPS spectra of GO and ODA-RGO. (c) Raman spectra of GO and ODA-RGO. (d) XRD curves of GO, ODA-RGO and graphite.

1724 cm^{-1} are from stretching vibrations of the C=C bonds and carboxylic groups, respectively. The characteristic bands of alkoxy and epoxide groups appear at 1225 cm^{-1} and 1057 cm^{-1}, respectively. It is proved that graphite has been oxidized to give GO, as evidenced by the existence of oxygen-containing functional groups. In FTIR spectrum of ODA-RGO, the absorption bands at 2920 cm^{-1}, 2848 cm^{-1} and 1460 cm^{-1} are related to the C–H stretching and bending vibrations of $-CH_2-$ groups. Besides, the absorption band at 1562 cm^{-1} corresponds to the coupling of N–H and C–N bonds, indicating the introduction of the long alkyl chain into GO nanosheets. Most of the characteristic bands of GO and ODA can be seen in the FTIR spectrum of ODA-RGO, but some related to oxides in GO disappear or is reduced due to the reduction.

The X-ray photoelectron spectroscopy (XPS) was adopted to further analyse the nanosheets. The C1s spectra of GO and ODA-RGO are shown in Fig. 1b. The C1s XPS spectrum of GO can be deconvoluted into four typical peaks: C–C (284.9 eV), C–O (286.9 eV), C=O (287.8 eV) and O–C=O (289.1 eV), indicating its high degree oxidation. The C1s XPS spectrum of ODA-RGO exhibits similar oxygen-containing functional group, however, having much weaker peak intensities, which indicates a considerable degree of deoxygenation after the chemical reduction. In addition, the C1s XPS spectra of ODA-RGO has an additional peak at 285.8 eV associated with C–N bonds. The XPS survey scan also shows an N1s peak at 400 eV for ODA-RGO (Fig. S1 in ESI†), and the C/O atomic ratios obviously increase from 2.67 to 18.99 after reduction (Table S1 in ESI†), which further confirm the successful of preparing ODA-RGO. Fig. 3c displays the Raman spectra of GO and ODA-RGO. The intensity ratio of the D peak to G peak in the Raman spectra is inversely proportional to in-plane crystalline sizes in graphite-based systems.[45,46] The value of $I_{(D)}/I_{(G)}$ increases from 2.40 to 2.96 after the chemical reduction, which indicates the partial recovery of the conjugated structure of graphene. The X-ray diffraction (XRD) curves obtained for GO, ODA-RGO and graphite are shown in Fig. 3d. The XRD curve of GO shows a peak centred at $2\theta = 10.52°$, corresponding to the (002) inter-planar spacing of 8.402 Å. The most intense peak of graphite at $2\theta = 26.56°$, corresponding to a *d*-spacing of 3.353 Å, is absent in the XRD pattern of GO. For ODA-RGO, a strong diffraction peak appears at $2\theta = 21.34°$, corresponding to a *d*-spacing of 4.160 Å. It indicates the extension of the inter-planar distance compared with graphite, which is caused by the grafting of ODA molecules onto RGO sheets *via* amidation.[36,38]

Fig. 2 gives TEM image of the ODA-RGO nanosheets. The wrinkled with sizes from several hundred nanometers to a few micrometers can be clearly seen from the image. It indicates the anisotropic mechanical properties of RGO sheets, *i.e.*, the in-plane rigidity and out-of-plane flexibility as well as folding ability, which are beneficial to follow the topological profiles of elastomer tools. As shown in the inset in Fig. 2, ODA-RGO can be stably dispersed in THF for several days, which is suitable for the following experiments.

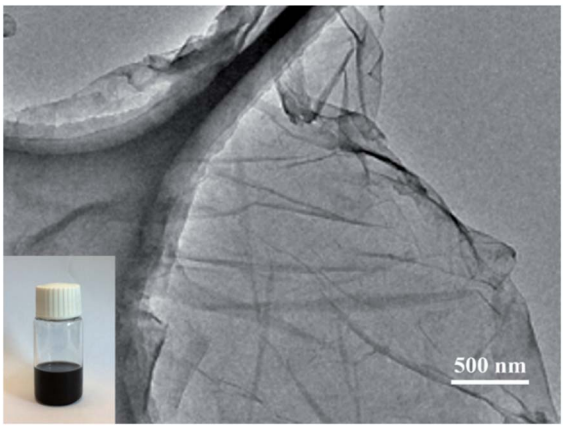

Fig. 2 TEM image of ODA-RGO. The inset shows ODA-RGO dispersion in THF (~4 mg mL^{-1}).

3.2 Fabrication of lotus-leaf-like surfaces

The soft-lithography was employed to duplicate the surface structures of lotus leaves to obtain the RGO-based superhydrophobic surfaces (Fig. 3). First, a piece of lotus leaf was used as a nature-created master to prepare the PDMS stamp through replica molding (Step a), where the PDMS prepolymer was cured at 50 °C for 6 h. After peeling off, the PDMS stamp negatively featured with the papillae on the lotus-leaf surface was obtained. Second, the ODA-RGO dispersion was cast on the surface of PDMS stamp through dropping and spreading. As the rapid volatilization of THF, a thin layer of concentrated "ink" covered the featured surface of the PDMS stamp (Step b). After that, the microcontact printing was performed by press the stamp on a piece of substrate (the glass slide or silicon wafer) (Step c). Finally, the lotus-leaf-like surface was formed on the substrate after peeling off the stamp and vacuum drying (Step d). As shown below, the lotus-leaf-like surface with superhydrophobic functions can be obtained by this procedure.

The lotus-leaf surfaces are covered by unique papillary structures with diameter and height both in ten-micron scale.[11–13] Through the replica molding, negative replica of the

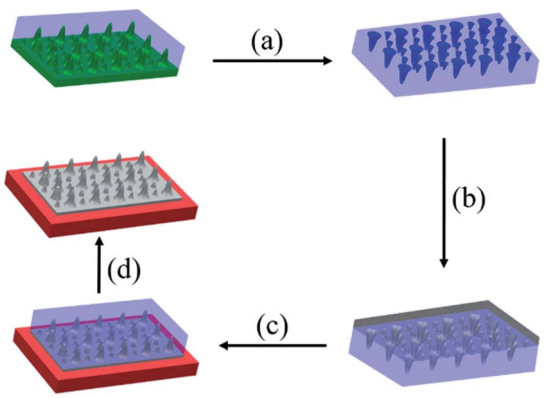

Fig. 3 Schematic diagram of the fabrication process of the ODA-RGO lotus-leaf-like surfaces, (a) preparation of the PDMS stamp through replica molding against a piece of fresh lotus leaf, (b) dropping the ODA-RGO dispersion on the PDMS stamp to form a thin layer of the "ink" on the surface, (c) pressing the "inked" stamp against the substrate for a few seconds, (d) peeling off the PDMS stamp and vacuum drying.

lotus-leaf surfaces was formed on the PDMS stamp. Optical microscope (OM) observation indicates that the micropores with diameters ranging from 5 to 10 μm are densely distributed on the PDMS stamp surfaces (Fig. 4a and b). These micropores are the negative duplicates of the papillae on the lotus leaf. It demonstrates that the lotus-leaf surface morphology is successfully duplicated from the lotus-leaf master to the PDMS stamp. After microcontact printing using the PDMS stamp and the ODA-RGO dispersion as the "ink", the lotus-leaf-like surfaces were obtained after vacuum drying. Fig. 4c and d show the surface structures of the printed layer on glass slide from OM observation. The structures with diameters ranging from 5 to 10 μm, corresponding to the papillae, can be clearly seen from the images. Other surface textures can also be seen from the images.

SEM observations can reveal more details of the PDMS stamp and lotus-leaf-like structures. Fig. 5 shows the SEM images of the PDMS stamp surface. It shows that the surface is covered with microscale pores and textures as the negative replicas of the lotus-leaf surfaces. The surface morphologies of the ODA-RGO layers formed by the drop-coating method with a dispersion of the same concentration on the substrate were observed with SEM first as a control (Fig. 6a1–a4). The rough relief-structures from the randomly stacking nanosheets can be seen only in the nanoscale. In the contrast, SEM observations clearly show that the mimicked papillary microstructures were formed on the printed ODA-RGO layers (Fig. 6b1–b4). A large number of the micro-papillae, with diameters ranging from 5 to 10 μm, heights ranging from 2 to 8 μm, exist on the surfaces. The distance between two nearest papillae is about 15 μm. Although the papillae are randomly distributed on the surface, the distance between two nearby papillae varies in a relatively narrow range. The average diameter and the distance between two papillae on the printed surface are close to those on fresh lotus-leaf surface, while the average height of the papillae on the printed layer is slightly reduced due to the evaporation of the dispersion medium. It is worthwhile to note that there are a large amount of wrinkles and crumpled nano-structures on the printed surface, which can be seen from both OM and SEM observations (Fig. 4c, d and 6b1–b4). Compared with the drop-coated ODA-RGO film (Fig. 6a1–a4), it can be concluded that in addition to the replication of the texture of the lotus leaf, the wrinkles on the surface are also from random stacking of the RGO nanosheets, which become crumpled during the contact printing and the drying process. This unique nanoscale roughness of the lotus-leaf-like surface made from RGO is distinct from the surfaces fabricated with polymers through soft-lithographic methods,[25,26] which is attributed to the rigidity of the 2D honeycomb carbon framework of RGO and the strong π–π stacking of the aromatic rings. This structural characteristic is beneficial to enhancing super-hydrophobicity of the surface as shown below.

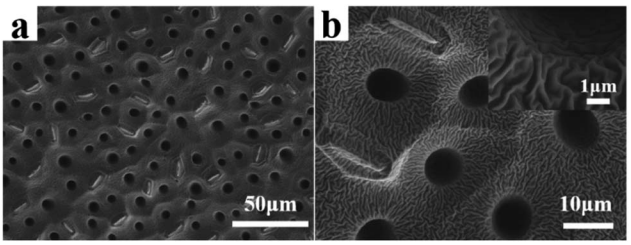

Fig. 5 SEM images of the surface structures on, (a) a PDMS stamp replicated from the lotus leaf, (b) magnified image of (a).

Surface roughness is one of the important factors affecting the surface hydrophobicity.[47,48] Fig. S2 (in ESI†) shows the 3D images of the drop-coated film surface and the printed lotus-leaf-like surface of ODA-RGO obtained from a confocal microscope system. The roughness values of the drop-coated film surface and the printed lotus-leaf-like surface of ODA-RGO on glass slides are 0.616 μm and 3.116 μm, respectively. The surface roughness of the printed lotus-leaf-like surface is obviously larger than that of the drop-coated film surface.

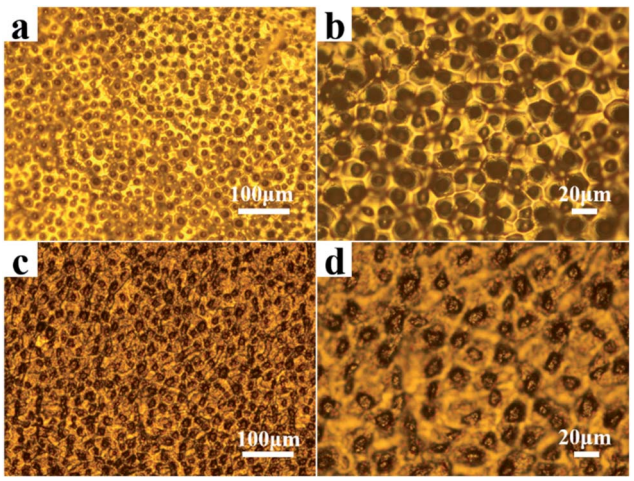

Fig. 4 Optical micrographs of the surface structures on, (a) a PDMS stamp replicated from the lotus leaf, (b) magnified image of (a), (c) printed lotus-leaf-like surface of ODA-RGO, (d) magnified image of (c).

3.3 Structure formation mechanism

The lotus-leaf-like structure formation through the contact printing process can be analysed as follows. PDMS stamp and its interaction with the surface and material play a key role for the soft-lithographic fabrication. Because of the low surface energy and mild curing condition, the PDMS stamp could well duplicate the nano/micro-structure on the lotus leaf and be easily peeled off from the surfaces with no damage to the fragile bio-surface. After dropping the "ink" on the surfaces of PDMS stamp, the ODA-RGO dispersion spreads and infiltrates into the pores on the stamp under capillary effect. With the quick volatilization of the solvent, the highly concentrated ODA-RGO layer covers the featured surface of the stamp. This process is similar to the contact printing with a polymer solution as the "ink".[49] When the PDMS stamp was pressed against the substrate surface, the ODA-RGO layer was transferred from the stamp surface to the substrate surface to form lotus-leaf-like structure on it. The transference of the ODA-RGO layer from

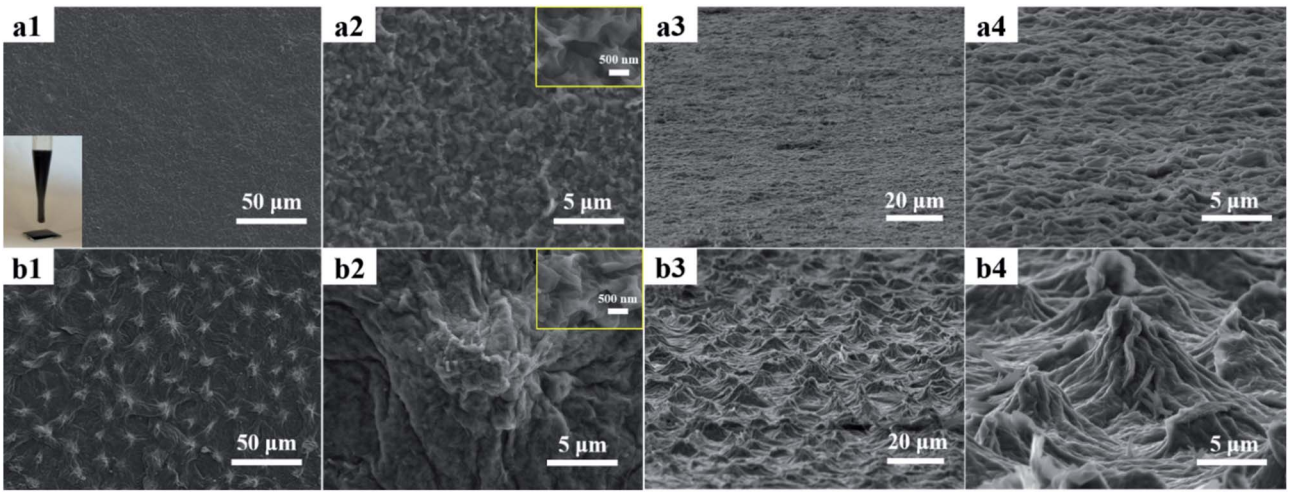

Fig. 6 Typical SEM images of the surface structures of ODA-RGO, (a1) a top-view image of the drop-coated film and the inset shows drop-coating method to coat the ODA-RGO dispersion on a glass slide, (a2) a magnified image of (a1) and the inset shows details, (a3) a side-view of the drop-coated film, (a4) a magnified image of (a3), (b1) a top-view image of the printed surface, (b2) a magnified image of (b1) and the inset gives the image of a single papilla, (b3) a side-view of the printed layer, (b4) a magnified image of (b3).

the stamp to the substrate is a critical step to form ODA-RGO lotus-leaf-like surface, which depends on the difference between the adhesion work values of two solid layers as estimated below.

The surface free energy of ODA-RGO, PDMS and the glass substrate was calculated by using Young–Dupré/Owens–Wendt equation.[50,51] The polar and non-polar contributions were obtained by the polar and dispersive components of two probe liquids and their contact angles using the following equation

$$\gamma_{lv}(1 + \cos\theta) = 2(\gamma_s^d\gamma_{lv}^d)^{0.5} + 2(\gamma_s^p\gamma_{lv}^p)^{0.5} \quad (1)$$

where γ_{lv} is the total surface energy of the probe liquid with the dispersive (γ_{lv}^d) and polar (γ_{lv}^p) components, γ_s^d and γ_s^p are the dispersive and polar components of the surface energy of the measured solid, θ is the contact angle between the probe liquid and the measured solid surface. To use this equation, the water and methylene iodide were selected as the probe liquids, whose values of γ_{lv}, γ_{lv}^d, γ_{lv}^p were obtained from the literature and listed in Table 1. The harmonic mean approximation method is used to estimate the values of the adhesion work between two solid layers,[52]

$$W_{12} = \frac{4\gamma_1^d\gamma_2^d}{\gamma_1^d + \gamma_2^d} + \frac{4\gamma_1^p\gamma_2^p}{\gamma_1^p + \gamma_2^p} \quad (2)$$

where W_{12} is the adhesion work between two solid layers, γ_1 and γ_2 are the surface free energy of the corresponding solids with the dispersive (γ_1^d, γ_2^d) and polar (γ_1^p, γ_2^p) components, respectively. The adhesion work of the ODA-RGO layer with the PDMS or glass slide were calculated by using above equations and the results are listed in Table 1. The value of adhesion work of the ODA-RGO layer on PDMS surface ($W_{\text{ODA-RGO/PDMS}} = 58.56$ mJ m^{-2}) is smaller than that on the glass slide ($W_{\text{ODA-RGO/Glass}} = 70.61$ mJ m^{-2}), which indicates the easy transference of the ODA-RGO layer from the PDMS stamp to the glass substrate. It is consistent with the observation of our experiment, which also shows that the ODA-RGO layer with the duplicated structures can stably adhere on the substrate. Moreover, the value of the adhesion work between two ODA-RGO layers equals 83.54 mJ m^{-2}, even larger than $W_{\text{ODA-RGO/Glass}}$, which ensures that the integrity of ODA-RGO lotus-leaf-like structures on the substrate.

3.4 Superhydrophobic properties

Fig. 7 shows water contact angles and digital photographs of the water droplets on both the drop-coated film surface and the printed lotus-leaf-like surface of ODA-RGO on glass slides. The contact angle (CA) is 96.9 ± 0.9° on the drop-coated film surface and 161.2 ± 1.7° on the lotus-leaf-like surface. As shown in Fig. 6a1–a4 and S2a (ESI†), the surfaces of the drop-coated film

Table 1 Surface tension of substrates and the adhesion work with ODA-RGO

	Contact angle (°)		Surface tension (mJ m^{-2})		Adhesion work (mJ m^{-2})
Substrate	H_2O	CH_2I_2	γ_s^p	γ_s^d	$W_{\text{ODA-RGO/substrate}}$
ODA-RGO	96.9	36.8	0.07	41.7	83.54
PDMS	110.5	71.1	0.04	22.5	58.56
Glass	15.1	35.4	41.1	30.4	70.61

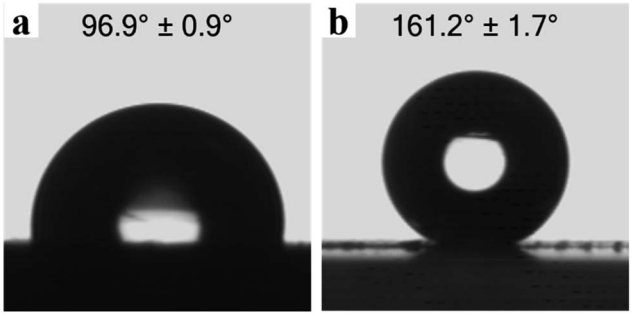

Fig. 7 Digital photographs of water droplets on, (a) a drop-coated surface of ODA-RGO, (b) a printed lotus-leaf-like surface of ODA-RGO.

only show the nanoscale roughness. Without the papillary structure, the ODA-RGO film is hydrophobic. On the other hand, with the formation of the lotus-leaf-like structures, the surface of the same material transforms from hydrophobic to super-hydrophobic with a water contact angle larger than 160°. This indicates that the lotus-leaf effect can increase the water CA for more than 60°. This behaviour can be understood by the some simplified model and theory, such as those proposed by Wenzel and Cassie,[53,54] as the surface roughness (Fig. S2b, in ESI†) is significantly increased. Deeper understanding of this effect can be reached by considering the contact line density criterion and asperity height criterion,[55] as well effects of topography length scales.[56] In this aspect, lotus leaf provides us with the master to have the optimized design by nature. As revealed by the SEM images given in Fig. 6b1–b4, the printed lotus-leaf-like surfaces also possess the nanoscale roughness due to the stacking of rigid RGO nanosheets, which is also beneficial to achieving the superhydrophobicity. As shown in the side-view image given in Fig. 6a3, the average film thickness prepared from the RGO dispersion is much larger than the height of the surface structures. Therefore, the effect of the substrate can be ignored for its contribution to the hydrophobicity.

The dynamic contact angle measurement was carried out to further characterize of the superhydrophobicity of the printed lotus-leaf-like surfaces. The contact angle hysteresis, defined as the difference between the advancing and receding water contact angles (θ_A and θ_R), is used to characterize the dynamic wettability.[56–58] Contact angle hysteresis arises from molecular interactions of the liquid with solid and surface roughness or heterogeneities. The contact angle hysteresis and the sliding angle (α), *i.e.* the minimum angle of tilt at which a droplet will spontaneously move has the following relationship

$$mg(\sin \alpha)/w = \gamma_{lv}(\cos \theta_R - \cos \theta_A) \quad (3)$$

where g is the force due to gravity, m and w are the mass and width of the droplet, γ_{lv} is the surface tension.[56] The small contact angle hysteresis means the easy for the droplet to slip away from the surface, which is critically important to characterize the super-hydrophobicity.[57,58] The measured values of the advancing and receding water contact angles of the lotus-leaf-like surface are 156.7° and 154.4°, respectively, (Fig. S3, in ESI†). The value of sliding angle (α) is calculated as 3.4° by eqn (3). Both the small contact angle hysteresis and the small sliding angle prove that the lotus-leaf-like surface of ODA-RGO has the dynamic superhydrophobicity. The above results obtained from the static and dynamic measurements indicate that the soft-lithographic duplication is a very effective approach to prepare the superhydrophobic surface.

3.5 Stability of the lotus-leaf-like surface

Superhydrophobic surfaces have found wide-range application in biotechnology, self-cleaning textiles and others.[1–4] However, the diverse environments, especially harsh conditions, will damage the surface structures and cause the loss of the super-hydrophobicity. To evaluate the environmental stability, the ODA-RGO super-hydrophobic surfaces were tested under different temperature and pH. The lotus-leaf-like surfaces show a stabilized superhydrophobicity after being subjected the temperature change in range from 40 to 150 °C. After being heated at each temperature for 24 h under vacuum and then cooled down to room temperature, the measured water CAs are all around 160 °C (Fig. 8a). The thermogravimetric analysis indicated that ODA-RGO does not show weight loss below 150 °C (Fig. S4 in ESI†). In addition, the SEM observations proved that the papillae and morphology of the lotus-leaf-like surface remain stable after being heat treatment at 150 °C for 24 (Fig. S5). To test the pH stability, the lotus-leaf-like surfaces were immersed in aqueous solutions with different pH ranging from 0 to 14 for 12 h, then repeatedly washed with ultrapure water and vacuum drying. After the treatment, the water CAs show a slight decrease, but all remain above 150° (Fig. 8b). The SEM observations show no obvious change of the papillary structures and morphology of the lotus-leaf-like surface (Fig. S6 in ESI†). These results indicate that the ODA-RGO lotus-leaf-like surfaces are stable for the super-hydrophobicity under conditions of the heating treatments and exposure to corrosive environment. On the other hand, the adhesion and abrasion resistance of the duplicated lotus-leaf-like structures are not satisfied. As discussed above, the adhesion work of the ODA-

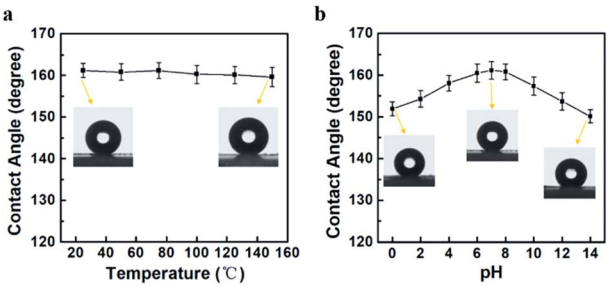

Fig. 8 The water contact angles of the ODA-RGO lotus-leaf-like surfaces after being treated at high temperature for 24 h or immersed in solutions with different pH for 12 h, (a) the relationship between the treating temperature and CA of the ODA-RGO lotus-leaf-like surface, (b) relationship between the solution pH value and CA of ODA-RGO lotus-leaf-like surface.

RGO layer with glass ($W_{ODA\text{-}RGO/Glass}$ = 70.61 mJ m^{-2}) is obviously smaller than that between two ODA-RGO layers (83.54 mJ m^{-2}). To improve the adhesion, an additional buffer layer with the high adhesion work to both the glass slide and ODA-RGO layer should be inserted during the preparation. To enhance the abrasion resistance and mechanical strength of the lotus-leaf-like structure, the cross-linking reaction between the RGO sheets can be introduced as reported in previous article.[59]

4 Conclusions

The RGO-based lotus-leaf-like surface was successfully fabricated through soft-lithographic duplication. In the process, the PDMS stamp was prepared by the replica molding against the surface of a fresh lotus leaf. The octadecylamine modified RGO (ODA-RGO) was prepared by grafting ODA onto GO nanosheets and chemical reduction at the same time in the suspension. After centrifugation and drying, ODA-RGO powder was then dispersed in THF to obtain the "ink". The lotus-leaf-like surfaces were obtained by microcontact printing using the PDMS stamp and ODA-RGO "ink". The duplicated lotus-leaf-like surface exhibits the high fidelity to the lotus-leaf surface, which is covered by papillae in micron-scale. Moreover, the in-plane rigidity and out-of-plane flexibility of RGO nanosheets afford the lotus-leaf-like surfaces with the roughness in the nanoscale. The as-prepared surfaces show superhydrophobicity with the water contact angle of 161.2 ± 1.7° and the difference between the advancing and the receding contact angles is less than 3°. The surfaces exhibit the stability of the superhydrophobicity after exposed to the high temperature for 24 h or solutions with different pH from 0 to 14 for 12 h. The RGO-based superhydrophobic surface with these superior properties through the scalable processing avenues are expected for applications in different areas.

Conflicts of interest

There are no conflicts of interest to declare.

Acknowledgements

This work was supported by the NSFC under project 51773108.

Notes and references

1 X. M. Li, D. Reinhoudt and M. Crego-Calama, *Chem. Soc. Rev.*, 2007, **36**, 1350–1368.
2 X. Guo and Z. Guo, *Langmuir*, 2019, **35**, 1047–1053.
3 M. F. Wang, N. Raghunathan and B. Ziaie, *Langmuir*, 2007, **23**, 2300–2303.
4 L. Feng, S. H. Li, Y. S. Li, H. J. Li, L. J. Zhang, J. Zhai, Y. L. Song, B. Q. Liu, L. Jiang and D. B. Zhu, *Adv. Mater.*, 2002, **14**, 1857–1860.
5 Y. Sun and Z. Guo, *Nanoscale Horiz.*, 2019, **4**, 52–76.
6 Y. Liu, N. Liu, Y. Jing, X. Jiang, L. Yu and X. Yan, *Colloids Surf., A*, 2019, **567**, 128–138.
7 H. Wang, C. Wang, S. Liu, L. Chen and S. Yong, *RSC Adv.*, 2019, **9**, 8569–8574.
8 J. Ge, D. Zong, Q. Jin, J. Yu and B. Ding, *Adv. Funct. Mater.*, 2018, **28**, 1705051.
9 R. Blossey, *Nat. Mater.*, 2003, **2**, 301–306.
10 M. B. Avinash, E. Verheggen, C. Schmuck and T. Govindaraju, *Angew. Chem., Int. Ed.*, 2012, **51**, 10324–10328.
11 M. Yamamoto, N. Nishikawa, H. Mayama, Y. Nonomura, S. Yokojima, S. Nakamura and K. Uchida, *Langmuir*, 2015, **31**, 7355–7363.
12 W. Barthlott and C. Neinhuis, *Planta*, 1997, **202**, 1–8.
13 C. Neinhuis and W. Barthlott, *Ann. Bot.*, 1997, **79**, 667–677.
14 H. Q. Li, Y. K. Lai, J. Y. Huang, Y. X. Tang, L. Yang, Z. Chen, K. Q. Zhang, X. C. Wang and L. P. Tan, *J. Mater. Chem. B*, 2014, **3**, 342–347.
15 W. Song, D. D. Veiga, C. A. Custódio and J. F. Mano, *Adv. Mater.*, 2009, **21**, 1830–1834.
16 F. Wang, S. Li and L. Wang, *Colloids Surf., A*, 2017, **513**, 389–395.
17 M. J. Hancock, K. Sekeroglu and M. C. Demirel, *Adv. Funct. Mater.*, 2012, **22**, 2223–2234.
18 X. Yao, Y. Song and L. Jiang, *Adv. Mater.*, 2011, **23**, 719–734.
19 Y. Qing, C. Long, K. An, C. Hu and C. Liu, *J. Colloid Interface Sci.*, 2019, **548**, 224–232.
20 Y. Xia and G. M. Whitesides, *Angew. Chem., Int. Ed.*, 1998, **37**, 550–575.
21 B. D. Gates, Q. Xu, M. Stewart, D. Ryan, C. G. Willson and G. M. Whitesides, *Chem. Rev.*, 2005, **105**, 1171–1196.
22 A. Taguchi, J. H. Smått and M. Lindén, *Adv. Mater.*, 2003, **15**, 1209–1211.
23 J. Sun, C. Yun, B. Cui, P. Li, X. Wang and F. Chu, *Polymers*, 2018, **10**, 1209.
24 J. Sun, Y. Guo, B. Cui, F. Chu, H. Li, Y. Li, M. He, D. Ding, R. Liu, L. Li and Y. Song, *Appl. Surf. Sci.*, 2018, **445**, 391–397.
25 M. H. Sun, C. X. Luo, L. P. Xu, H. Ji, Q. Ouyang, D. P. Yu and Y. Chen, *Langmuir*, 2005, **21**, 8978–8981.
26 B. Liu, Y. N. He, F. Yin and X. G. Wang, *Macromol. Rapid Commun.*, 2006, **27**, 1859–1864.
27 K. S. Novoselov, A. K. Geim, S. V. Morozov, D. Jiang, Y. Zhang, S. V. Dubonos, I. V. Grigorieva and A. A. Firsov, *Science*, 2004, **306**, 666–669.
28 A. K. Geim and K. S. Novoselov, *Nat. Mater.*, 2007, **6**, 183–191.
29 M. J. Allen, V. C. Tung and R. B. Kaner, *Chem. Rev.*, 2010, **110**, 132–145.
30 S. Stankovich, D. A. Dikin, G. H. B. Dommett, K. M. Kohlhaas, E. J. Zimney, E. A. Stach, R. D. Piner, S. B. Nguyen and R. S. Ruoff, *Nature*, 2006, **442**, 282–286.
31 D. A. Dikin, S. Stankovich, E. J. Zimney, P. D. Piner, G. H. B. Dommett, G. Evmenenko, S. B. Nguyen and R. S. Ruoff, *Nature*, 2007, **448**, 457–460.
32 S. J. Park and R. S. Ruoff, *Nat. Nanotechnol.*, 2009, **4**, 217–224.
33 G. Eda and M. Chhowalla, *Adv. Mater.*, 2010, **22**, 2392–2415.
34 K. P. Loh, Q. L. Bao, G. Eda and M. Chhowalla, *Nat. Chem.*, 2010, **2**, 1015–1024.
35 C. Cheng and D. Li, *Adv. Mater.*, 2013, **25**, 13–30.

36 S. Stankovich, D. A. Dikin, R. D. Piner, K. A. Kohlhaas, A. Kleinhammes, Y. Jia, Y. Wu, S. T. Nguyen and R. S. Rouff, *Carbon*, 2007, **45**, 1558–1565.
37 D. R. Dreyer, S. Park, C. W. Bielawski and R. S. Rouff, *Chem. Soc. Rev.*, 2010, **39**, 228–240.
38 Z. Y. Xiong, C. L. Liao and X. G. Wang, *J. Mater. Chem. C*, 2015, **3**, 6224–6231.
39 M. J. Nine, M. A. Cole, D. N. H. Tran and D. Losic, *J. Mater. Chem. A*, 2015, **3**, 12580–12602.
40 D. Prasai, J. C. Tuberquia, R. R. Harl, G. K. Jennings and K. I. Bolotin, *ACS Nano*, 2012, **6**, 1102–1108.
41 Z. Y. Xiong, X. W. Yun, B. Tang and X. G. Wang, *Carbon*, 2016, **107**, 548–556.
42 X. W. Yun, Z. Y. Xiong, L. Tu, L. Bai and X. G. Wang, *Carbon*, 2017, **125**, 308–317.
43 G. X. Wang, X. P. Shen, B. Wang, J. Yao and J. Park, *Carbon*, 2009, **47**, 1359–1364.
44 G. Wang, J. Yang, J. Park, X. Gou, B. Wang, H. Liu and J. Yao, *J. Phys. Chem. C*, 2008, **112**, 8192–8195.
45 A. C. Ferrari and J. Robertson, *Phys. Rev. B*, 2000, **61**, 14095–14107.
46 K. N. Kudin, B. Ozbas, H. C. Schniepp, R. K. Prud'homme, I. A. Aksay and R. Car, *Nano Lett.*, 2008, **8**, 36–41.
47 M. Miwa, A. Nakajima, A. Fujishima, K. Hashimoto and T. Watanabe, *Langmuir*, 2000, **16**, 5754–5760.
48 D. Quéré, *Annu. Rev. Mater. Res.*, 2008, **38**, 71–99.
49 B. Liu, M. Q. Wang, Y. N. He and X. G. Wang, *Langmuir*, 2006, **22**, 7405–7410.
50 D. K. Owens and R. C. Wendt, *J. Appl. Polym. Sci.*, 1969, **13**, 1741–1747.
51 M. E. Schrader, *Langmuir*, 1995, **11**, 3585–3589.
52 S. Wu, *J. Adhes.*, 1973, **5**, 39–55.
53 R. N. Wenzel, *Ind. Eng. Chem.*, 1936, **28**, 988–994.
54 A. B. D. Cassie and S. Baxter, *Trans. Faraday Soc.*, 1944, **40**, 546–551.
55 C. W. Extrand, *Langmuir*, 2004, **20**, 5013–5018.
56 D. Öner and T. J. MaCarthy, *Langmuir*, 2000, **16**, 7777–7782.
57 W. Chen, A. Y. Fadeev, M. C. Hsieh, D. Öner, J. Youngblood and T. J. McCarthy, *Langmuir*, 1999, **15**, 3395–3399.
58 C. W. Extrand, *Langmuir*, 2003, **19**, 3793–3796.
59 Z. Y. Xiong, T. H. Gu and X. G. Wang, *Langmuir*, 2014, **30**, 522–532.

